Journal of Biomedical Optics

BiomedicalOptics.SPIEDigitalLibrary.org

Optical catapulting of microspheres in mucus models—toward overcoming the mucus biobarrier

Ada-Ioana Bunea
Manto Chouliara
Stine Harloff-Helleberg
Andrew R. Bañas
Einstom L. Engay
Jesper Glückstad

SPIE.

Ada-Ioana Bunea, Manto Chouliara, Stine Harloff-Helleberg, Andrew R. Bañas, Einstom L. Engay, Jesper Glückstad, "Optical catapulting of microspheres in mucus models—toward overcoming the mucus biobarrier," *J. Biomed. Opt.* **24**(3), 035001 (2019), doi: 10.1117/1.JBO.24.3.035001.

Optical catapulting of microspheres in mucus models—toward overcoming the mucus biobarrier

Ada-Ioana Bunea,[a] Manto Chouliara,[a] Stine Harloff-Helleberg,[b] Andrew R. Bañas,[a] Einstom L. Engay,[a] and Jesper Glückstad[a,c,*]
[a]Technical University of Denmark, DTU Fotonik, Department of Photonics Engineering, Kongens Lyngby, Denmark
[b]University of Copenhagen, Department of Pharmacy, Faculty of Health and Medical Sciences, Copenhagen, Denmark
[c]OptoRobotix Aps, Frederiksberg, Denmark

Abstract. The generalized phase contrast method is employed as an efficient "phase-only" laser beam-shaping technique in an optical setup built for catapulting microspheres through simple mucus models. The influence of the laser power and mucin concentration on the motion of the microspheres is investigated in terms of instant and average velocities on a 250-μm trajectory, corresponding to the mucus thickness in the human gastrointestinal tract. Increasing the laser power leads to higher velocities in all the tested samples, while increasing the mucin concentration leads to significant velocity decrease for similar laser input power. However, velocities of up to 95 $\mu m \cdot s^{-1}$ are demonstrated in a 5% mucin simple mucus model using our catapulting system. This study contributes to understanding and overcoming the challenges of optical manipulation in mucus models. This paves the way for efficient optical manipulation of three-dimensional-printed light-controlled microtools with the ability to penetrate the mucus biobarrier for *in vitro* drug-delivery studies. [DOI: 10.1117/1.JBO.24.3.035001]

Keywords: optical catapulting; generalized phase contrast; particle tracking; mucus model; light robotics.

Paper 180459RR received Jul. 20, 2018; accepted for publication Jan. 21, 2019; published online Mar. 1, 2019.

1 Introduction

Oral delivery of certain biopharmaceuticals would have an outstanding societal influence, as it should increase patient convenience and compliance. In addition to countless existing formulations, new highly selective and potent drug candidates have entered advanced clinical trials in recent years, providing significant momentum for oral drug delivery. One of the main challenges in the field is that the intestine secretes mucus, which constitutes a natural biobarrier rather impermeable to a large number of compounds.[1–3] Hence, thorough understanding of how biopharmaceuticals interact with and are transported across mucus and epithelial barriers is of utmost importance.

Mucus is a hydrogel that contains a mixture of mucins as the principal dry weight component, typically 2% to 5% (w/v), and low amounts of other proteins and lipids.[4] Mucins are high-molecular weight glycoproteins that can be either secreted or membrane-bound. Mucus protects the epithelium from pathogens, toxins, and endogenous substances such as hydrochloric acid, pepsin, and other digestive enzymes, while allowing the exchange of nutrients.[5] The heterogeneity of mucus compositions from different species, individuals, and situses is a challenge for developing appropriate research models of mucus biobarriers. For example, in humans, the thickness of the mucus layer throughout the gastrointestinal tract varies between 10 and 250 μm.[6] Due to the variable length of the glycoprotein chains, the mesh-spacing heterogeneity of mucus pores is also high, varying from 100 nm to several μm.[4]

Different research studies attempt to mimic mucus composition to various degrees, with the simplest viable model for mucus biobarriers being aqueous mucin solutions based on dehydrated porcine gastric mucin (PGM).[7] Rehydrated PGM dispersions mimic mucus biobarrier properties only to a certain extent, and their rheological properties do not match those of native mucus.[8] However, in addition to the pore structure and viscoelastic properties of native mucus, which are important for size filtering, the mucus mesh also performs interaction filtering on the basis of physicochemical properties[9] through, e.g., hydrogen bonding, hydrophobic or ionic interactions.[10] Although aqueous PGM dispersions are a simplistic model of the mucus biobarrier, they are widely used due to the availability of PGM and its physicochemical properties that closely resemble those of human mucins.[11,12] PGM-based simple mucus models facilitate investigation of the interaction filtering properties of human mucus biobarriers.

Overcoming the mucus biobarrier for drug delivery has been attempted with the aid of different vector carriers, such as mucoadhesive micro- and nanoparticles,[13,14] mucus-penetrating nanoparticles[15] and liposomes,[16] or cell-penetrating peptides.[17] Improving the efficiency of drug carriers for delivery across mucus biobarriers is generally achieved through controlling the interaction with mucus by engineering the carriers to have either mucoadhesive or mucus-penetrating properties.[18,19] Chitosan and hyaluronic acid are often used as mucoadhesive coatings.[20] Poly(ethylene glycol) is widely used for "stealth" surface modification,[21–24] and other candidates as mucus-penetrating coatings have recently been reviewed.[25] Understanding the interactions between coated particles and mucus biobarriers can help design efficient drug carriers for inhalation,[26] ocular,[20] transnasal,[27] vaginal,[28] and oral[16,29] administration.

Arthur Ashkin's first report of optical trapping described how a microsphere hit with a milliwatt power beam will be "accelerated in the direction of the light."[30] Since then, optical

*Address all correspondence to Jesper Glückstad, E-mail: jesper.gluckstad@fotonik.dtu.dk

forces have been employed for actuating microscopic particles for various applications.[31–34] For example, optical tweezers are particularly useful for single molecule measurements,[35–37] while optical catapulting is more commonly used for particle sorting[38] and aerosol analysis.[39] Beam shaping allows improved control over how the optical forces are applied and interact with the microparticles.[40] Whereas actuation typically relies on gradient forces to attract a particle toward a similarly moving light distribution, other applications benefit more from optical scattering forces that effectively push or catapult a particle along a predefined light path.

As a method to extend our understanding of the physicochemical interactions occurring within mucus, we demonstrate the feasibility of optically catapulting microstructures as means to investigate the biobarrier. Such dynamic experiments should complement existing methods based on tracking particles undergoing passive diffusion[41,42] and thus allow a more thorough study of the interaction filtering properties of mucus, which would then facilitate the screening of different coatings for improved drug delivery through mucus. We have recently reported functionalization of three-dimensional (3-D) printed microstructures for this purpose.[43] Finding the best coating should eventually allow us to develop 3-D printed light-actuated microtools[44–48] with the ability to carry biopharmaceuticals through the mucus biobarrier for *in vitro* drug delivery tests.

2 Materials and Methods

2.1 *Catapulting Particles with Generalized Phase Contrast*

Our setup for catapulting microspheres benefits from an extended working distance made possible by using low numerical aperture (NA) objectives.[49–51] Using counter-propagating catapulting beams, it has also been demonstrated that such low NA setups can actuate microstructures by transversely translating and adjusting the relative intensities of the beam pairs.[49–51] Low NA objectives allow the light to interact with the sample environment in a wider, 3-D manner, which will allow us in the future to perform advanced studies using different microtools.[45,48] Furthermore, this extended geometry facilitates the extraction of z-depth information through direct side-view imaging. These features come at the price of typically having a smaller back aperture in the low NA objective lenses used. In commonly used holographic optical tweezers,[52] a wider back aperture (higher NA) is necessary to get a wider conjugate image of the spatial light modulator (SLM) through the aperture. The generalized phase contrast (GPC) method circumvents these NA constraints through the use of a "4f" imaging geometry. This means that a localized focused light distribution is situated at the objective lens's back aperture, and hence, potential losses from aperture truncation are minimized. Similar to diffractive holography, GPC is also an efficient "phase-only" laser beam-shaping technique.[53,54] However, unlike in diffractive holography, GPC-shaped beams have a well-defined extended region where the beam intensity is more uniform, speckle-free, and with well-defined boundaries. The uniform lateral beam profile of GPC-shaped beams results in a relatively extended axial profile as the beam propagates, which improves the optical catapulting of microspheres over long distances.

The GPC method works by transforming an incident Gaussian beam into desired output shapes, such as a top-hat, through a direct mapping of the input phase mask patterns.[55] To produce a desired output intensity shape, an input phase mask is visualized at the output plane as an intensity distribution through common path interference with a synthesized reference wave (SRW). The SRW is brought about by a phase-contrast filter (PCF) that usually applies a 180-deg phase shift to the beam's lower spatial frequency components. Unlike in the case of using a Gaussian beam, a microsphere being catapulted by a GPC-shaped beam receives a uniformly intense radiation flux over its cross section. A schematic of the GPC light-shaping method is illustrated in Fig. 1.

When optically catapulting microspheres over an extended distance, it is desirable to have a beam distribution that remains relatively localized as it propagates. A well-known example of a beam with extended propagation is a Bessel beam.[56] However, in order to efficiently generate a Bessel beam, an axicon phase distribution must be generated using a freeform refractive optical element or an extra SLM, which would increase the cost of the optical setup. Furthermore, the energy in the intense area of the Bessel beam is only half of the energy available, as the other half is spread throughout the periphery and accounts for the "reconstructed light" in subsequent planes. Despite having a relatively shorter propagation distance where the beam is localized, compared to a Bessel beam, GPC is more effective in utilizing the available light, with an energy efficiency of about

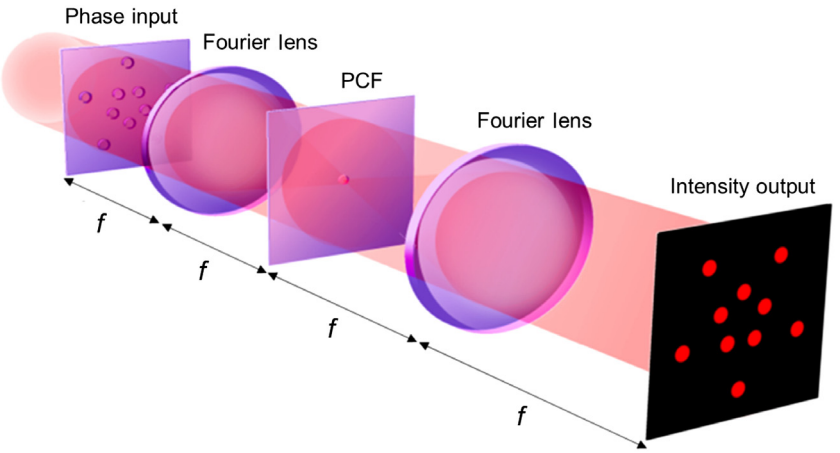

Fig. 1 Schematic diagram of the GPC light shaping method.

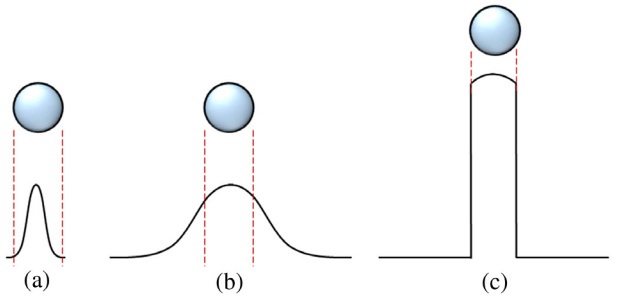

Fig. 2 Typical configurations at which a microsphere and beam can overlap. In (a), the majority of the light's intensity is incident at the particle, but is significantly lower toward the edges of the particle. The incident light distribution in (b) is more uniform; however, energy outside the particle's boundaries is wasted. In (c), the incident light intensity is more uniform, while also preventing energy waste. GPC light shaping (c) provides 3× higher intensity on the particle compared to (b) for the same beam input power.

84%.[55] Furthermore, instead of a freeform refractive optical element or an additional SLM, GPC requires simple binary phase masks, which are easier to fabricate.

Figure 2 illustrates different scenarios for how a microsphere and beam can overlap. The distributions in Figs. 2(a) and 2(b) represent different magnifications of a typical Gaussian, Airy-disk or other focal spot distribution characterized by a gradual intensity roll-off. Figure 2(c) represents a sharply bounded top-hat that can be generated by GPC. In Fig. 2(c), the light incident at the microsphere is more evenly distributed compared to that in Fig. 2(a), while also being more confined to the microsphere compared to the case in Fig. 2(b). As the beam gets narrower in Fig. 2(a), this configuration also approaches that of an optical tweezer that has a shorter manipulation range and will rather attract instead of catapulting the microsphere. When using GPC to generate a top-hat as in Fig. 2(c), the setup requires about a third of the power, compared to the case in Fig. 2(b), for generating the same intensity level.[55] Combined with the relatively uniform light intensity distribution on the microsphere, this efficiency advantage is why GPC was selected as a light-shaping method in this study.

A typical GPC-generated output beam has a characteristic top-hat field profile characterized by a sharp change in intensity at its boundaries. However, as the beam propagates, this profile changes due to diffraction as shown in Fig. 3.[57] Despite this change in radiation profile, the beam intensity remains relatively localized when compared to a typical Gaussian or Airy-disk focal spot generated from a similar optical setup. Hence, a more consistent amount of scattering force pushes the microsphere as it traverses in the axial direction. This makes it ideal for catapulting microspheres over a longer distance.[47,55,57,58] Although it is also possible to extend the propagation of Gaussian or Airy-disk beams by modifying the setup's magnification, such an expanded beam would lead to a less efficient system, having more energy falling outside the microsphere's cross-sectional area.

Simulated propagations of a GPC-generated top-hat and a similarly confined Gaussian beam are shown in Fig. 3. The simulation emulates practical scenarios wherein all the optical energy overlaps with the microsphere [as in Figs. 2(a) and 2(a)] and scaled to match the parameters used in our experiment. Hence, we chose a GPC disk radius that matches the microsphere's radius and a Gaussian waist that is one-third of the microsphere radius (and also one-third of the GPC disk radius). It can be seen that the GPC beam diverges more slowly than the narrow Gaussian and therefore provides more consistent force to a microsphere moving along the axial direction.

The effective force components acting on a spherical particle, which are typically in the order of piconewtons, were investigated by Rodrigo et al.[57] These forces depend on the light intensity distribution, the refractive indices of the host medium and the particle, and on the fact that the refraction angle is higher at the edges of the particle than at its center. We are expecting that the densest light intensity distribution will take place at the beginning of the microspheres' movement, where the spatial distribution is closer to the ideal top-hat. As a microsphere is moving upward inside the chamber, the light intensity incident to it is gradually decreasing, which should lead to a deceleration of the microsphere due to opposing forces, such as gravity and drag forces.

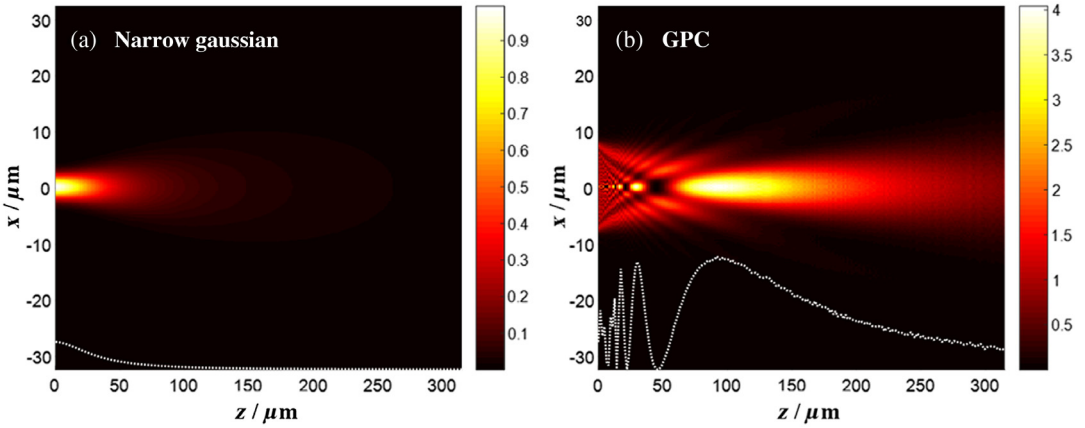

Fig. 3 Pseudocolor plot of the xz-plane intensity distribution appearing at $z > 0$ (arbitrary units) for a typical focused Gaussian and GPC-generated beam directed toward the positive z-axis.[57] The Gaussian and GPC profiles were set in the simulation so that their energy falls within the same microsphere region. Due to the subsequent focusing with GPC, the color bars are scaled differently to keep the features visible.

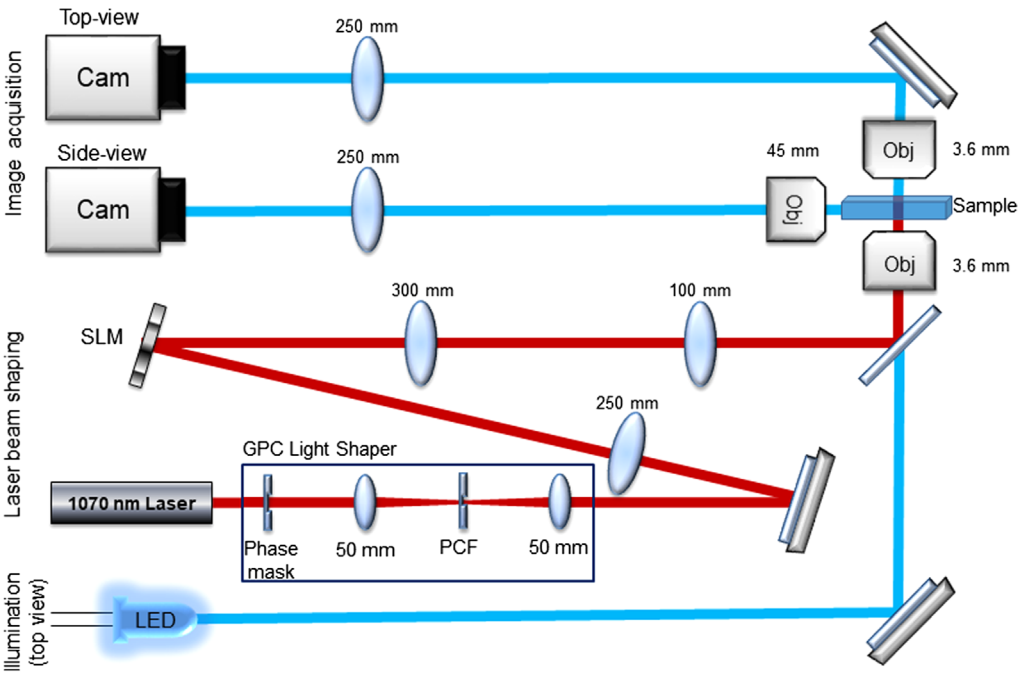

Fig. 4 Schematic diagram of the setup for catapulting experiments. Illumination for side-view imaging was achieved with the aid of a portable light source placed near the sample (not included in the diagram).

2.2 *Optical Catapulting Experimental Setup*

In order to investigate the movement of the microspheres inside the mucin solutions, the setup in Fig. 4 was constructed. A 1070-nm laser (IPG Photonics, Massachusetts) shaped by a GPC system was used to catapult the microspheres. An LCoS type SLM (Hamamatsu Photonics, Japan) with 800×600 pixels with a pixel pitch of 20 μm was used to actuate the shaped GPC output via a "Holo-GPC" configuration.[59] Holo-GPC works by multiplexing speckle-free GPC top-hats into holographically distributed 3-D locations in the sample volume by utilizing the convolution principle.[53,60] Hence, having Holo-GPC available is convenient for addressing multiple microspheres over a wide-working volume. The measurements in this paper, however, were performed on individual microspheres, which means that the method is equally applicable if standard GPC, without the holographic multiplexing, is used. Hence, despite having an SLM in the setup, the catapulting experiments reported herein did not take advantage of this.

The laser was demagnified to have a 1-mm diameter, which matches a prefabricated GPC light shaper.[61] The GPC light shaper used two Fourier lenses ($f = 50$ mm) to form a $4f$ configuration, and had a circular phase mask with a diameter of 0.39 mm, and a PCF with a 38-μm phase-shifting radius. The Fourier transform of the illuminated phase mask was expanded onto the SLM by 5× by placing a lens ($f = 250$ mm) after the light shaper. The distribution at the SLM was subsequently demagnified onto the back aperture of the objective lens by 1/3× using a pair of lenses ($f_1 = 300$ mm and $f_2 = 100$ mm).

Two objective lenses ($f = 3.6$ mm, NA = 0.55) were used to image the GPC disks onto the sample and for the top view and a third objective lens ($f = 45$ mm, NA = 0.1) for the side camera. The resulting disk after the $f = 3.6$ mm objective lens had a calculated diameter of ~17 μm, which closely matches the 15-μm diameter of the microspheres. The longer focal length and the working distance of the side-view objective leave enough clearance from the measurement cuvette and the top and bottom objectives. Although the relevant data were obtained through side-view imaging, the top view was necessary for alignment of the system and ensuring that the beam was aimed at the microspheres to be catapulted.

2.3 *Mucin Preparation*

The microspheres to be optically catapulted were suspended in varying concentrations of PGM (type II, Sigma Aldrich cat. no. M2378) prepared in HEPES (Sigma-Aldrich Denmark A/S, cat. no. H0887, pH 7.0-7.6) containing Tween 80 (MP Biomedicals, California, cat. no. 02103170). A 10-mM HEPES buffer was prepared by diluting the 1 M HEPES stock in millipore water (18.2 MΩ · cm at 25°C). For all experiments, the mucin solutions were prepared by adding mucin to the 10-mM HEPES buffer and allowing it to rehydrate for 20 min at room temperature under mixing at 300 rpm using an IKA RH basic two magnetic stirrer. About 0.1% Tween 80 was added to the samples used in rheology measurements. About 0.1% Tween 80 and 1.5% of 15 μm polybead polystyrene microspheres (Polysciences Inc., Pennsylvania) were added to the mucin dispersions for optical catapulting experiments. The refractive index of the solutions was measured and can be considered constant, as the difference between millipore water and the 5% mucin concentration medium is below 1%.

2.4 *Rheology Measurements*

The effect of mucin concentration on viscosity was evaluated using an ARES-G2 rheometer (TA Instruments, New Castle, Delaware), equipped with a peltier plate and truncated cone (1 deg, 40 mm from TA Instruments, New Castle, Delaware), and the temperature was set to 21°C. To prevent evaporation during measurements, a solvent trap cover was used

(TA Instruments, New Castle, Delaware). Test samples were carefully pipetted to the center of the peltier plate, and proper sample distribution and subsequent equilibration were ensured by a conditioning step with pre-shear set to 10 Pa followed by an equilibrium step of 5 min at 21°C. Subsequently, a steady state flow step was carried out by applying a shear rate of 10 to 5000 s^{-1}, conducting three consecutive measurements of 10 s each, allowing a maximum of 5% variance, collecting four points per decade. All samples were measured in triplicate ($n = 3$). Statistical analysis of the rheological data was done via a one-way analysis of variance using GraphPad Prism version 7.0b (GraphPad Software, San Diego, California).

The viscoelastic behavior of the 5% mucin samples was not characterized. These concentrated samples precipitated during the conditioning step, leading to an obvious phase separation.

2.5 *Optical Catapulting Experiments*

For each set of measurements, 15-μm diameter polystyrene microspheres were placed along with a mucin solution inside the 250×250 μm^2 square channel (Fig. 5) from a quartz cuvette (Hellma GmbH, Germany). The microspheres rapidly sedimented on the bottom of the microchannel. The system was then aligned to focus on one randomly selected microsphere for catapulting. The height of the measurement channel was chosen to match the thickness of the mucus layer in the human digestive tract.[6] The videos were recorded using laser powers (as set on the laser source) of 0.20, 0.50, 1, 1.50, and 1.80 W and mucin concentrations of 0.1%, 0.25%, 0.5%, 1%, 3%, and 5%. This allowed us to investigate the effect on increasing laser powers on catapulting the microspheres in relation to the different mucin concentrations.

2.6 *Microsphere Tracking and Data Analysis*

The motion of the microspheres was captured with a point gray camera at 10 fps. The Manual Tracking plugin designed by Fabrice P. Cordelières for the ImageJ software[62] was used for tracking the microspheres for all the experiments. The accuracy of the tracking is limited by the pixel size of the recorded videos to ~0.1 μm. The microspheres were tracked from the first frame in which they rise above the lower cuvette wall until the last frame just before reaching the upper cuvette wall (a distance corresponding to ~250 μm, as defined by the chamber height). The "instantaneous" velocities of the microspheres (for the shortest observable time intervals of 0.1 s, as determined by the frame rate) were computed in the software and either used as such (denoted as instant velocities) or averaged for the entire trajectory (denoted as average velocities). Recordings where a second microsphere interfered with the catapulting were excluded from the analysis. The trajectories of 10 microspheres from five different samples were analyzed for every mucin concentration and catapulting laser power.

The motion of microspheres in 3% mucin using 0.2 W input laser power was extremely slow, which would cause significant errors in tracking due to subpixel size displacements in between consecutive frames, and thus it was excluded from the data analysis. In 5% mucin, an input laser power of 0.2 W was not sufficient to push the microspheres upward.

The sensitivity of the system in terms of its ability to respond to perturbations caused by the presence of mucin is given by the slope of the linear fit passing through the origin in the velocity versus laser power plots. This parameter was calculated from both the average and maximum instant velocities and is given in $\mu m \cdot s^{-1} \cdot W^{-1}$).

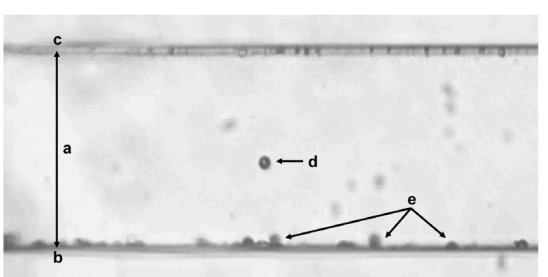

Fig. 5 Bright field image of a microsphere being catapulted inside millipore water taken with the side-view camera. a: Measurement cuvette containing microspheres mixed in mucin dispersion; b: lower cuvette wall; c: upper cuvette wall; d: microsphere being catapulted; e: other microspheres lying on the bottom of the measurement cuvette. The microspheres have a diameter of 15 μm. The visible top (c) and bottom (b) inner walls of the cuvette are 250-μm apart.

3 Results and Discussion

3.1 *Viscoelastic Behavior of Mucin Samples*

As it can be seen in Fig. 6, the viscoelastic behavior of samples containing low concentrations of mucin (up to 0.25%) is very similar to that of buffer (no statistical differences). This indicates that in these samples, the glycoprotein chains do not form a detectable network of secondary interactions, most likely due to the too large distances between the mucin fragments.

The samples with mucin concentrations between 0.5% and 3% behave in similar manner and are characterized by increased viscosity and a changed viscoelastic behavior (shear thinning) compared to buffer. This indicates the formation of a viscoelastic network. Based on these results, the critical concentration for the formation of a viscoelastic network in our experimental conditions should be between 0.25% and 0.5% mucin.

3.2 *Catapulting in Water*

In order to ensure that our setup allows reproducible measurements, we initially conducted a series of experiments using a "blank" sample without mucin, which contained millipore

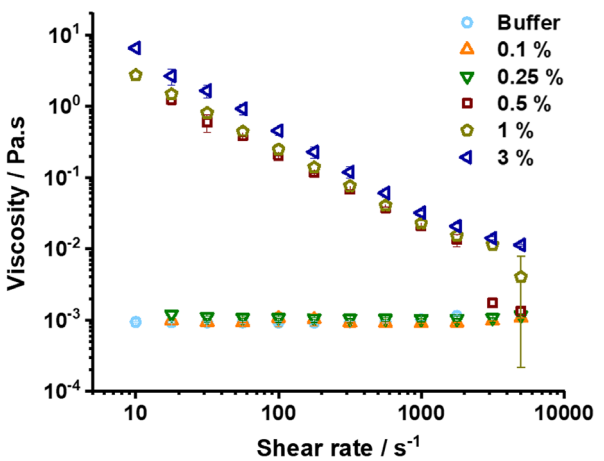

Fig. 6 Rheological characterization of samples ($n = 3$) containing different mucin concentrations.

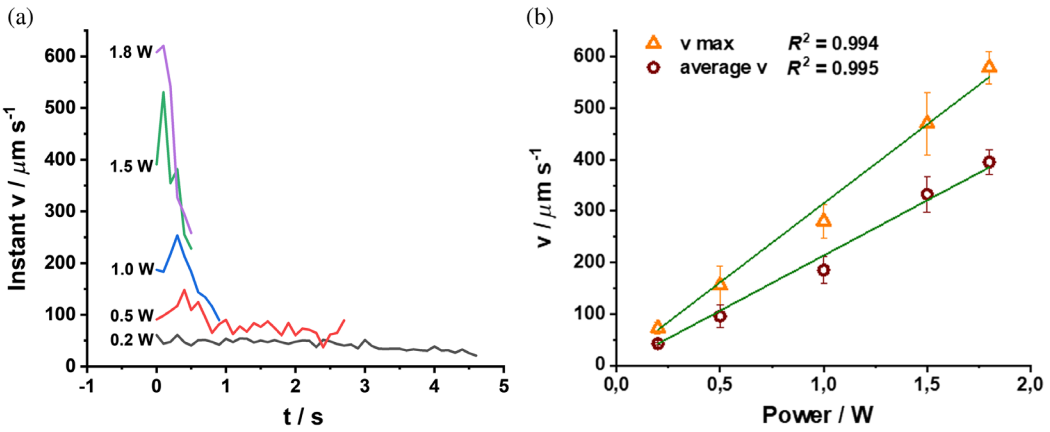

Fig. 7 Tracking results in water samples containing Tween 80 ($n = 10$): (a) instant velocities as a function of time for different laser powers and (b) maximum and average velocities as a function of laser power.

water, 0.1% Tween 80 and 1.5% of 15 μm polystyrene microspheres.

The instantaneous, average, and maximum velocities of the microspheres in water are shown in Fig. 7. The system is optimized such that the GPC disks are formed at the lower wall of the measurement chamber, where the microspheres are also lying, and thus provides an optimal overlap with the GPC disks in the beginning of the microsphere trajectories. However, due to the axially changing intensity distribution of GPC-shaped beams (Fig. 3), there is an initial "slowness" in the microsphere motion and the highest velocities are achieved a fraction of a second after the microspheres start being pushed by the laser beam, after the microsphere goes past the more intense region of the beam. The local intensity maxima before the broad intense region (Fig. 3) could also be causing weak gradient forces that initially attract the microsphere. As the microspheres move vertically through the measurement chamber, their speed is decreasing sensibly, which is to be expected, as described in Sec. 2.1. This decrease as the microspheres are catapulted further from the image plane of the GPC beam is more obvious at high laser powers (1.5 and 1.8 W), as it can be observed in Fig. 7(a). At low laser powers (0.2 and 0.5 W), the frame-to-frame displacement of the microspheres is of only several pixels, which causes the calculated instant velocity signal to be noisy and makes the velocity decrease less observable.

A comparison between different input powers for catapulting in water is shown in Video 1. The microsphere displacement 0.5 s after turning on the laser beam can be seen in Fig. 8(a).

3.3 *Catapulting in Mucin*

In order to understand how the presence of short mucin glycoprotein chains affects the ability to catapult microspheres in our system, we investigated aqueous dispersions containing 0.1% to 5% mucin. Among these, the 3% and 5% aqueous mucin dispersions can be considered simple mucus models due to the similarity with the 2% to 5% mucin content of native mucus.

A comparison between different input powers for catapulting in 1% mucin is shown in Video 2. The microsphere displacement 1 s after turning on the laser beam can be seen in Fig. 8(b).

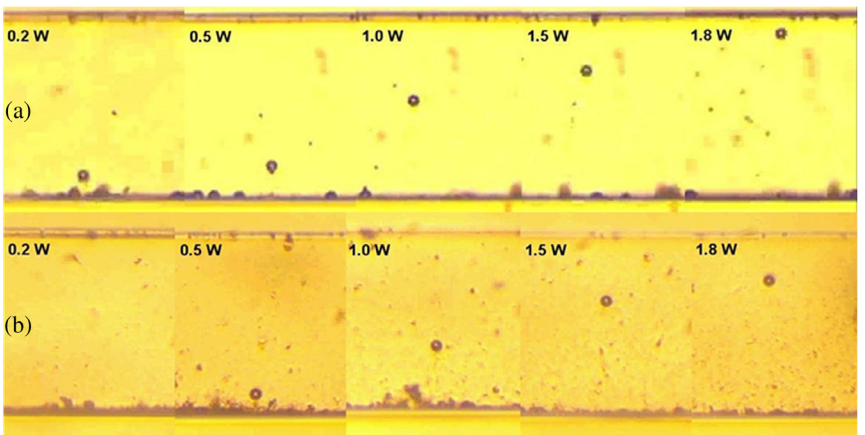

Fig. 8 Comparison of optical catapulting of polystyrene microspheres using different input laser powers in (a) water (Video 1) and (b) 1% mucin (Video 2). The frames shown correspond to (a) 0.5 s and (b) 1 s after turning on the laser beam for catapulting. (Video 1, MP4, 0.5 MB[URL: https://doi.org/10.1117/1.JBO.24.3.035001.1].; Video 2, MP4, 2.3 MB[URL: https://doi.org/10.1117/1.JBO.24.3.035001.2].).

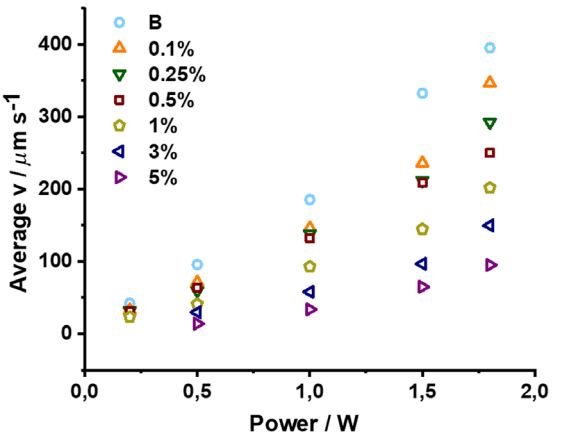

Fig. 9 Average velocities ($n = 10$) at different laser powers and different mucin concentrations. "B" is a blank sample containing 0.1% Tween 80 in millipore water.

The experimental results obtained using different laser powers in aqueous mucin dispersions with concentrations up to 5% are presented in Fig. 9. Each experimental data point was calculated by averaging the velocity of 10 microspheres. The average values, including standard deviations, are given in Sec. 5.

As it can be seen in Fig. 9, increasing the laser power leads to a velocity increase for all tested samples. On the other hand, the average velocities of the microspheres decrease as the mucin concentration increases. This is an anticipated behavior due to the biobarrier properties of mucus, which the mucin dispersions replicate to some extent. The velocity decrease can be attributed to a combined effect of altered light propagation in mucin dispersions and to physicochemical interactions between the polystyrene microspheres and the simple mucus model. Polystyrene surfaces are slightly charged and hydrophobic,[63] with loose polymer chains present at the interface.[64] Thus, it is to be expected that the polystyrene microspheres employed in our study can lead to hydrophobic interactions[65] with the mucin fragments.

The sensitivity of the system (calculated from both instant and average velocities) decreases exponentially as the mucin concentration increases, as shown in Fig. 10. This shows that

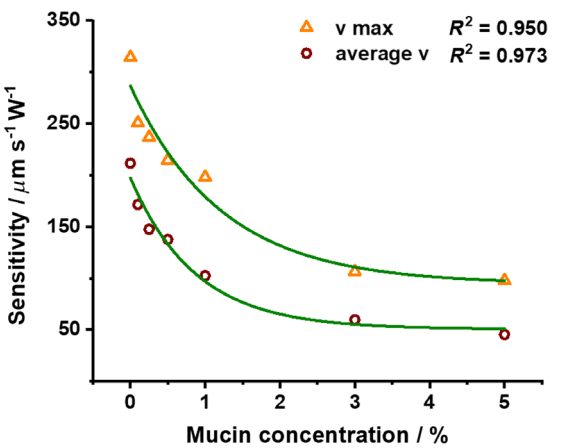

Fig. 10 Sensitivity decrease of the system at increasing mucin concentrations. The sensitivity values were calculated from both the average and maximum velocities versus laser power plots.

the addition of mucin glycoprotein chains in low concentrations (0.1% to 1%) significantly changes the behavior of the microspheres, which can be partly attributed to the physicochemical interactions between the polystyrene microspheres and the mucin fragments. The addition of low amounts of mucin does not change the viscoelastic behavior, but it can already lead to hydrophobic interactions between the microspheres and the sample. Beyond 0.5% mucin, the glycoprotein fragments assemble in a viscoelastic network. This can explain why further increasing the mucin concentration has a lower effect on the sensitivity.

4 Conclusions

To the best of our knowledge, this work is the first to study the laser catapulting of microspheres as a means to investigate a model mucus biobarrier. The influence of the laser power and mucin concentration on the microsphere motion was investigated and analyzed. To ensure catapulting over a relatively long (250 μm) distance, similar to the thickness of mucus in the human digestive tract, we used the GPC light-shaping method, which has been previously tested in extended geometries. The setup was developed to allow beam shaping using Holo-GPC, which can be used in future studies for simultaneously catapulting multiple microspheres.

The setup demonstrated optical manipulation of the microspheres through solutions with high mucin concentrations using input laser powers as low as 0.5 W. As expected, increasing the mucin concentration led to a decrease in microsphere velocity, while increasing the laser power for a given mucin solution lead to an increase in microsphere velocities. Our system for optical catapulting allows us to push polystyrene microspheres through the simple mucus model investigated. In the future, particles with different shapes and surface chemistry can be compared in this setup to gather information about the physicochemical interactions between such particles and their environment. This suggested approach can complement existing methods that study such interactions by offering the user control over the dynamic testing conditions through simply adjusting the input laser power.

Understanding optical manipulation in mucus models is vital for future biomedical applications of light-controlled microparticles for *in vitro* drug delivery tests. In order to attempt drug delivery through mucus biobarriers using light-actuated microtools, optical manipulation needs to be optimized to accommodate the requirements of both light-control and handling biological samples. Precise optical manipulation, can be better achieved using increased laser irradiation, but there is an inherent need to minimize the applied laser intensity to avoid photodamage of biological samples. Our findings will support further investigation of overcoming the mucus biobarrier for biopharmaceutical applications using light-controlled particles with different surface properties and light-actuated microtools.

5 Appendix

Table 1 shows the average values (n=10), including standard deviations, of microspheres catapulted in simple mucus models with different mucin concentrations using different input laser powers.

Table 1 Average velocities ($n = 10$) in $\mu m \cdot s^{-1}$ of microspheres for different input laser powers and mucin concentrations.

	0.2 W	0.5 W	1 W	1.5 W	1.8 W
Buffer	42.1 ± 1.9	95.6 ± 22.0	185.5 ± 25.4	332.6 ± 34.9	395.3 ± 23.6
0.1% mucin	32.5 ± 6.2	71.1 ± 5.5	146.0 ± 29.0	235.9 ± 49.0	346.7 ± 46.0
0.25% mucin	32.1 ± 4.6	59.6 ± 18.6	138.4 ± 28.5	212.0 ± 34.1	292.4 ± 21.9
0.5% mucin	31.4 ± 3.5	63.9 ± 3.5	132.5 ± 11.0	208.7 ± 25.0	250.0 ± 42.7
1% mucin	23.4 ± 6.0	41.1 ± 5.3	92.7 ± 18.5	144.8 ± 22.2	201.9 ± 15.7
3% mucin	N/A	29.9 ± 3.4	58.0 ± 8.1	96.7 ± 9.7	150.0 ± 23.0
5% mucin	N/A	13.9 ± 1.4	33.8 ± 3.9	64.9 ± 12.8	95.1 ± 23.4

Disclosures

The authors declare that there are no conflicts of interest related to this article.

Acknowledgments

The authors acknowledge financial support from the Novo Nordisk Foundation (Grand Challenge Program, NNF16OC0021948) and VILLUM FONDEN (Research Grant No. 00022918).

References

1. L. Wu et al., "Engineering nanomaterials to overcome the mucosal barrier by modulating surface properties," *Adv. Drug Delivery Rev.* **124**, 150–163 (2018).
2. C. Menzel and A. Bernkop-Schnürch, "Enzyme decorated drug carriers: targeted swords to cleave and overcome the mucus barrier," *Adv. Drug Delivery Rev.* **124**, 164–174 (2018).
3. J. Leal, H. D. C. Smyth, and D. Ghosh, "Physicochemical properties of mucus and their impact on transmucosal drug delivery," *Int. J. Pharm.* **532**(1), 555–572 (2017).
4. M. Boegh and H. M. Nielsen, "Mucus as a barrier to drug delivery—understanding and mimicking the barrier properties," *Basic Clin. Pharmacol. Toxicol.* **116**(3), 179–186 (2015).
5. R. A. Cone, "Barrier properties of mucus," *Adv. Drug Delivery Rev.* **61**, 75–85 (2009).
6. M. García-Díaz et al., "The role of mucus as an invisible cloak to transepithelial drug delivery by nanoparticles," *Adv. Drug Delivery Rev.* **124**, 107–124 (2018).
7. J. Y. Lock, T. L. Carlson, and R. L. Carrier, "Mucus models to evaluate the diffusion of drugs and particles," *Adv. Drug Delivery Rev.* **124**, 34–49 (2018).
8. J. Kočevar-Nared, J. Kristl, and J. Šmid-Korbar, "Comparative rheological investigation of crude gastric mucin and natural gastric mucus," *Biomaterials* **18**(9), 677–681 (1997).
9. O. Lieleg and K. Ribbeck, "Biological hydrogels as selective diffusion barriers," *Trends Cell Biol.* **21**(9), 543–551 (2011).
10. S. P. Authimoolam and T. D. Dziubla, "Biopolymeric mucin and synthetic polymer analogs: their structure, function and role in biomedical applications," *Polymers* **8**(3), 71 (2016).
11. J. Perez-Vilar and R. L. Hill, "The structure and assembly of secreted mucins," *J. Biol. Chem.* **274**, 31751–31754 (1999).
12. G. E. Yakubov et al., "Molecular structure and rheological properties of short-side-chain heavily glycosylated porcine stomach mucin," *Biomacromolecules* **8**(11), 3467–3477 (2007).
13. M. Sakagami et al., "Mucoadhesive beclomethasone microspheres for powder inhalation: their pharmacokinetics and pharmacodynamics evaluation," *J. Control. Release* **80**(1–3), 207–218 (2002).
14. M. Moreno-Sastre et al., "Pulmonary drug delivery: a review on nanocarriers for antibacterial chemotherapy," *J. Antimicrob. Chemother.* **70**(11), 2945–2955 (2015).
15. S. K. Lai, Y.-Y. Wang, and J. Hanes, "Mucus-penetrating nanoparticles for drug and gene delivery to mucosal tissues," *Adv. Drug Delivery Rev.* **61**(2), 158–171 (2009).
16. X. Li et al., "Novel mucus-penetrating liposomes as a potential oral drug delivery system: preparation, in vitro characterization, and enhanced cellular uptake," *Int. J. Nanomed.* **6**, 3151–3162 (2011).
17. M. Kristensen and H. M. Nielsen, "Cell-penetrating peptides as carriers for oral delivery of biopharmaceuticals," *Basic Clin. Pharmacol. Toxicol.* **118**(2), 99–106 (2016).
18. K. Maisel et al., "Effect of surface chemistry on nanoparticle interaction with gastrointestinal mucus and distribution in the gastrointestinal tract following oral and rectal administration in the mouse," *J. Control. Release* **197**, 48–57 (2015).
19. E. M. Pridgen, F. Alexis, and O. C. Farokhzad, "Polymeric nanoparticle drug delivery technologies for oral delivery applications," *Expert Opin. Drug Delivery* **12**(9), 1459–1473 (2015).
20. M. M. Silva et al., "Chitosan nanoparticles as a mucoadhesive drug delivery system for ocular administration," *Mar. Drugs* **15**(12), 370 (2017).
21. S. K. Lai et al., "Rapid transport of large polymeric nanoparticles in fresh undiluted human mucus," *Proc. Natl. Acad. Sci. U.S.A.* **104**(5), 1482–1487 (2007).
22. Y.-Y. Wang et al., "Addressing the PEG mucoadhesivity paradox to engineer nanoparticles that 'slip' through the human mucus barrier," *Angew. Chem. Int. Ed.* **47**(50), 9726–9729 (2008).
23. J. M. Newby et al., "Technological strategies to estimate and control diffusive passage times through the mucus barrier in mucosal drug delivery," *Adv. Drug Delivery Rev.* **124**, 64–81 (2018).
24. E. A. Nance et al., "A dense poly(ethylene glycol) coating improves penetration of large polymeric nanoparticles within brain tissue," *Sci. Transl. Med.* **4**(149), 149ra119 (2012).
25. V. V. Khutoryanskiy, "Beyond PEGylation: alternative surface-modification of nanoparticles with mucus-inert biomaterials," *Adv. Drug Delivery Rev.* **124**, 140–149 (2018).
26. C. S. Schneider et al., "Nanoparticles that do not adhere to mucus provide uniform and long-lasting drug delivery to airways following inhalation," *Sci. Adv.* **3**(4), e1601556 (2017).
27. Y. Wang et al., "Mucoadhesive and enzymatic inhibitory nanoparticles for transnasal insulin delivery," *Nanomedicine* **9**(4), 451–464 (2014).
28. B. Martínez-Pérez et al., "Controlled-release biodegradable nanoparticles: from preparation to vaginal applications," *Eur. J. Pharm. Sci.* **115**, 185–195 (2018).
29. L. M. Ensign, R. Cone, and J. Hanes, "Oral drug delivery with polymeric nanoparticles: the gastrointestinal mucus barriers," *Adv. Drug Delivery Rev.* **64**(6), 557–570 (2012).
30. A. Ashkin, "Acceleration and trapping of particles by radiation pressure," *Phys. Rev. Lett.* **24**(4), 156–159 (1970).
31. A. Ashkin, "Applications of laser radiation pressure," *Science* **210**(4474), 1081–1088 (1980).

32. A. Jonáš and P. Zemánek, "Light at work: the use of optical forces for particle manipulation, sorting, and analysis," *Electrophoresis* **29**(24), 4813–4851 (2009).
33. O. M. Maragò et al., "Optical trapping and manipulation of nanostructures," *Nat. Nanotechnol.* **8**(11), 807–819 (2013).
34. S. E. S. Spesyvtseva and K. Dholakia, "Trapping in a material world," *ACS Photonics* **3**(5), 719–736 (2016).
35. K. Dholakia, P. Reece, and M. Gu, "Optical micromanipulation," *Chem. Soc. Rev.* **37**, 42–55 (2008).
36. D. G. Grier, "A revolution in optical manipulation," *Nature* **424**(8), 810–816 (2003).
37. E. A. Abbondanzieri et al., "Direct observation of base-pair stepping by RNA polymerase," *Nature* **438**(7067), 460–465 (2005).
38. I. Perch-Nielsen et al., "Parallel particle identification and separation for active optical sorting," *J. Opt. A* **11**(3), 034013 (2009).
39. F. J. Fortes, L. M. Cabalín, and J. J. Laserna, "Laser-induced breakdown spectroscopy of solid aerosols produced by optical catapulting," *Spectrochim. Acta Part B* **64**(7), 642–648 (2009).
40. M. Woerdemann et al., "Advanced optical trapping by complex beam shaping," *Laser Photonics Rev.* **7**(6), 839–854 (2013).
41. W. Shan et al., "Overcoming the diffusion barrier of mucus and absorption barrier of epithelium by self-assembled nanoparticles for oral delivery of insulin," *ACS Nano* **9**(3), 2345–2356 (2015).
42. B. S. Schuster et al., "Particle tracking in drug and gene delivery research: state-of-the-art applications and methods," *Adv. Drug Delivery Rev.* **91**, 70–91 (2015).
43. A.-I. Bunea et al., "Optimization of 3D-printed microstructures for investigating the properties of the mucus biobarrier," *Micro Nano Eng.* **2**, 41–47 (2019).
44. J. Glückstad et al., "Light-actuated microrobots for biomedical science," *SPIE Newsroom* (2017).
45. M. J. Villangca et al., "Light-driven micro-tool equipped with a syringe function," *Light Sci. Appl.* **5**(9), e16148 (2016).
46. D. Palima and J. Glückstad, "Gearing up for optical microrobotics: micromanipulation and actuation of synthetic microstructures by optical forces," *Laser Photonics Rev.* **7**(4), 478–494 (2013).
47. J. Glückstad and D. Palima, *Light Robotics: Structure-Mediated Nanobiophotonics*, Elsevier, Amsterdam (2017).
48. E. Engay et al., "Natural convection induced by an optically fabricated and actuated microtool with a thermoplasmonic disk," *Opt. Lett.* **43**(16), 3870–3873 (2018).
49. V. R. Daria et al., "Optimizing the generalized phase contrast method for a planar optical device," *J. Opt. A* **5**(5), S211–S215 (2003).
50. M. J. Villangca et al., "Generalized phase contrast-enhanced diffractive coupling to light-driven microtools," *Opt. Eng.* **54**(11), 111308 (2015).
51. R. L. Eriksen, P. C. Mogensen, and J. Glückstad, "Demonstration of ternary-phase-array illumination based on the generalised phase contrast method," *Opt. Commun.* **202**, 37–45 (2002).
52. D. G. Grier and Y. Roichman, "Holographic optical trapping," *Appl. Opt.* **45**(5), 880–887 (2006).
53. A. Bañas and J. Glückstad, "Light shaping with holography, GPC and holo-GPC," *Opt. Data Process. Storage* **3**(1), 20–40 (2017).
54. D. Palima et al., "Generalized phase contrast matched to Gaussian illumination," *Opt. Express* **15**(19), 11971–11977 (2007).
55. A. Bañas et al., "GPC light shaper for speckle-free one- and two- photon contiguous pattern excitation," *Opt. Express* **22**(5), 5299–5311 (2014).
56. J. Durnin, "Exact solutions for nondiffracting beams. I. The scalar theory," *J. Opt. Soc. Am. A* **4**(4), 651–654 (1987).
57. P. J. Rodrigo, I. R. Perch-Nielsen, and J. Glückstad, "Three-dimensional forces in GPC-based counterpropagating-beam traps," *Opt. Express* **14**(12), 5812–5822 (2006).
58. H.-U. Ulriksen et al., "Independent trapping, manipulation and characterization by an all-optical biophotonics workstation," *J. Eur. Opt. Soc.* **3**, 08034 (2008).
59. D. Palima et al., "Alternative modes for optical trapping and manipulation using counter-propagating shaped beams," *J. Opt.* **13**(4), 044013 (2011).
60. A. Bañas and J. Glückstad, "Holo-GPC: holographic generalized phase contrast," *Opt. Commun.* **392**, 190–195 (2017).
61. A. Bañas et al., "GPC light shaper: static and dynamic experimental demonstrations," *Opt. Express* **22**(20), 23759–23769 (2014).
62. C. A. Schneider, W. S. Rasband, and K. W. Eliceiri, "NIH image to ImageJ: 25 years of image analysis," *Nat. Methods* **9**(7), 671–675 (2012).
63. E. Thormann et al., "Interactions between a polystyrene particle and hydrophilic and hydrophobic surfaces in aqueous solutions interactions between a polystyrene particle and hydrophilic and hydrophobic surfaces in aqueous solutions," *Langmuir* **24**(6), 7278–7284 (2008).
64. T. Kajiyama, K. Tanaka, and A. Takahara, "Surface molecular motion of the monodisperse polystyrene films," *Macromolecules* **30**(2), 280–285 (1997).
65. A. Faghihnejad and H. Zeng, "Hydrophobic interactions between polymer surfaces: using polystyrene as a model system," *Soft Matter* **8**(9), 2746–2759 (2012).

Ada-Ioana Bunea has a PhD in micro- and nanotechnology from the Technical University of Denmark (DTU) and is currently leading a project on BioBots, light robotics microtools applied in biological samples. Originally trained as a chemist at the University of Bucharest, in Romania, her background is highly interdisciplinary, combining fabrication, surface modification, and characterization techniques.

Stine Harloff-Helleberg is trained as a pharmacist from the University of Copenhagen and received her PhD in food biophysics from SCIENCE, University of Copenhagen. Based on her highly interdisciplinary background, her current research focuses on design and development of novel and innovative drug delivery systems for oral delivery of biopharmaceuticals, e.g., peptides and proteins. Her primary focus is barrier interactions between the mucosal barrier and advanced drug delivery systems.

Einstom L. Engay is currently pursuing his PhD project in nanobiophotonics for light robotics at the Technical University of Denmark. He received his BSc degree in applied physics and his MSc degree in physics from the University of the Phillippines Diliman. His main interests are in the fields of optical manipulation, beam-shaping, and plasmonics.

Jesper Glückstad established Programmable Phase Optics in Denmark and has published 300+ journal and conference papers and holds 30+ patents. He obtained his PhD from the Niels Bohr Institute in 1994 and his Doctor of Science in 2004. He is inventor of GPC and its holographic extensions, pioneered Light Robotics and published two books on these topics. He cofounded OptoRobotix ApS in Silicon Valley in 2011 and is a fellow of both OSA and SPIE.

Biographies of the other authors are not available.